



Liquefaction phenomena associated with the Emilia earthquake sequence of May–June 2012 (Northern Italy)

Emergo Working Group: G. Alessio, L. Alfonsi, C. A. Brunori, P. Burrato, G. Casula, F. R. Cinti, R. Civico, L. Colini, L. Cucci, P. M. De Martini, E. Falcucci, F. Galadini, G. Gaudiosi, S. Gori, M. T. Mariucci, P. Montone, M. Moro, R. Nappi, A. Nardi, R. Nave, D. Pantosti, A. Patera, A. Pesci, G. Pezzo, M. Pignone, S. Pinzi, S. Pucci, S. Salvi, C. Tolomei, P. Vannoli, A. Venuti, and F. Villani

Istituto Nazionale di Geofisica e Vulcanologia, Via di Vigna Murata, 605, 00143 Rome, Italy

Correspondence to: S. Pucci (stefano.pucci@ingv.it)

Received: 25 July 2012 – Published in Nat. Hazards Earth Syst. Sci. Discuss.: –

Revised: 9 November 2012 – Accepted: 11 December 2012 – Published: 18 April 2013

Abstract. In this paper we present the geological effects induced by the 2012 Emilia seismic sequence in the Po Plain. Extensive liquefaction phenomena were observed over an area of $\sim 1200 \text{ km}^2$ following the 20 May, M_L 5.9 and 29 May, M_L 5.8 mainshocks; both occurred on about E–W trending, S dipping blind thrust faults. We collected the coseismic geological evidence through field and aerial surveys, reports from local people and Web-based survey. On the basis of their morphologic and structural characteristics, we grouped the 1362 effects surveyed into three main categories: liquefaction (485), fractures with liquefaction (768), and fractures (109). We show that the quite uneven distribution of liquefaction effects, which appear concentrated and aligned, is mostly controlled by the presence of paleo-riverbeds, out-flow channels and fans of the main rivers crossing the area; these terrains are characterised by the pervasive presence of sandy layers in the uppermost 5 m, a local feature that, along with the presence of a high water table, greatly favours liquefaction. We also find that the maximum distance of observed liquefaction from the earthquake epicentre is $\sim 30 \text{ km}$, in agreement with the regional empirical relations available for the Italian Peninsula. Finally, we observe that the contour of the liquefaction observations has an elongated shape almost coinciding with the aftershock area, the InSAR deformation area, and the $I \geq 6$ EMS area. This observation confirms the control of the earthquake source on the liquefaction distribution, and provides useful hints in the characterisation of the seismogenic source responsible for historical and pre-historical liquefactions.

1 Introduction

In May–June 2012, a seismic sequence struck a broad area of the Emilia-Romagna region in Northern Italy (Fig. 1), resulting in 26 fatalities and hundreds of injured, 15 000 homeless, severe damage of historical centres and industrial areas, and an estimated economic toll of ~ 2 billion euros. The sequence included two mainshocks. The first one occurred on 20 May at 02:03 UTC with a M_L 5.9 ($44^\circ 53' 23''$, $11^\circ 13' 47''$, $h = 6.3 \text{ km}$; ISIDE Database, 2012), hit in an area between Finale Emilia and San Felice sul Panaro; the second occurred on 29 May at 07:00 UTC with a M_L 5.8 ($44^\circ 51' 03''$, $11^\circ 05' 09''$, $h = 10.2 \text{ km}$; ISIDE Database, 2012), 12 km southwest of the previous mainshock (Fig. 2). Notably, the second shock determined the definitive collapse of many buildings already weakened. The whole aftershocks area extended in an E–W direction for more than 50 km, and included five $M_L \geq 5.0$ events and more than 1800 $M_L > 1.5$ events (Fig. 2). The focal mechanisms of the main events (Fig. 2) consistently show a compressional kinematics with E–W oriented nodal planes (dip 50° – 60° N and 30° – 40° S; Pondrelli et al., 2012; Scognamiglio et al., 2012; TDMT Database, 2012). These mechanisms are consistent with a horizontal, N–S oriented compression (P-axes) defined also by present-day stress indicators in the region (Montone et al., 2012 and references therein; Fig. 1) and by the GPS-derived velocity field (Devoti et al., 2011).

The epicentral area of the 2012 Emilia sequence falls in the southern part of the Po Plain, $\sim 40 \text{ km}$ north of the foothills of the northern Apennines thrust and fold mountain belt

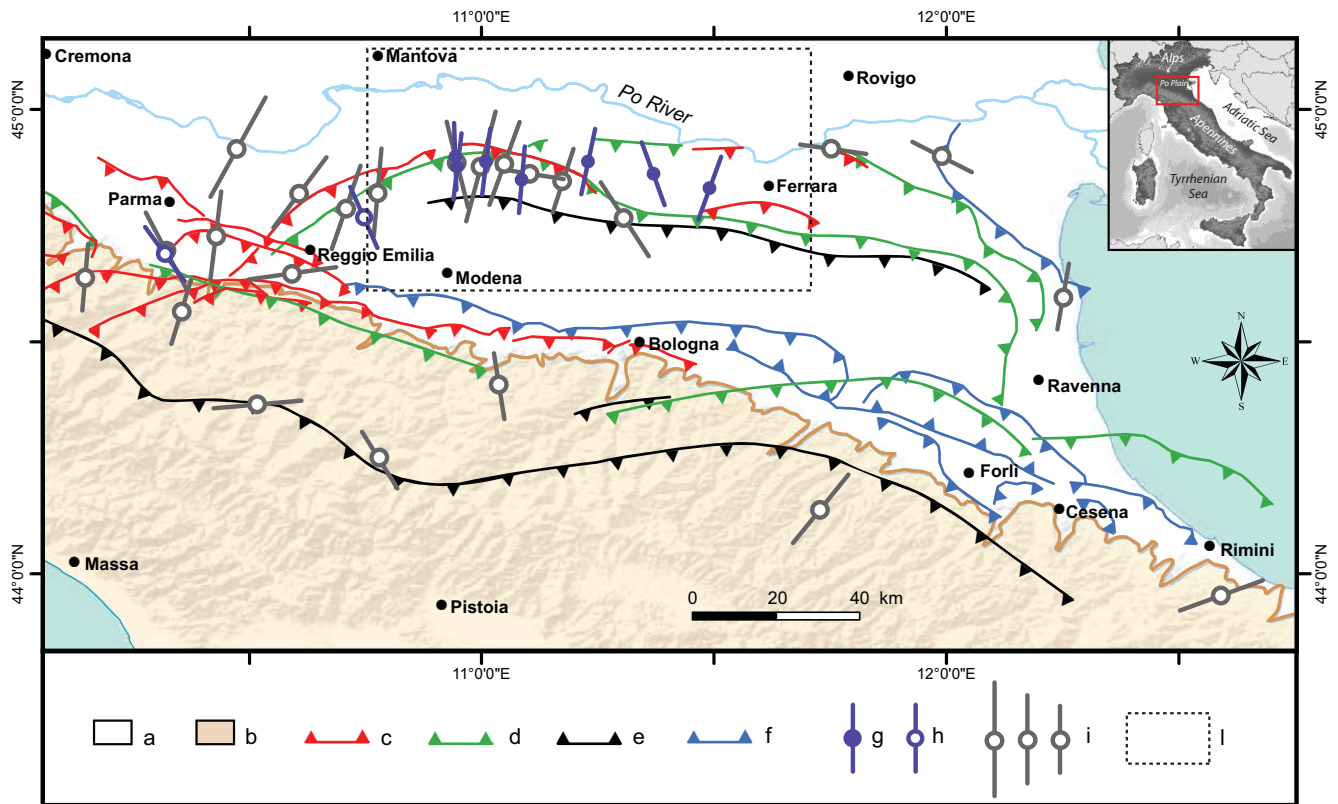


Fig. 1. Schematic structural setting of the southern Po Plain (main buried structures after Boccaletti and Martelli, 2004) with orientation of maximum horizontal stress from focal mechanisms of the Emilia 2012 earthquake sequence (Scognamiglio et al., 2012) and from the Italian present-day stress map (Montone et al., 2012). (a) Po Plain units (Plio–Quaternary); (b) Apenninic Units (Meso–Cenozoic); (c) active and recent (< 1 My) shallow thrusts; (d) active and recent thrust fronts in the Meso–Cenozoic carbonatic sequence; (e) active and recent thrust fronts in the basement; (f) reactivated thrust fronts of the Pliocene–Early Pleistocene (4.5–1 My); (g) maximum horizontal stress orientation from earthquake focal mechanisms of $M \geq 5.0$ events of the Emilia 2012 sequence; (h) maximum horizontal stress orientation from past earthquakes (M_w 5.0 Parma 1983 and M_w 5.4 Reggio Emilia 1996); (i) maximum horizontal stress orientation from borehole breakouts (scaled by quality); (l) area of Fig. 2.

(Figs. 1 and 2). This portion of the Apennines is characterised by N- and NE-verging thrusts and folds, involving both the terrigenous sedimentary cover and the carbonate Mesozoic sequences resulting from the late Oligocene–Quaternary compressional tectonic phases (i.e. Ghelardoni, 1965; Pieri and Groppi, 1981). The external fronts of the northern Apennines accretionary prism, namely from W to E, the Monferato, Emilia, and Ferrara–Romagna arcs, are buried beneath a cover of Pliocene hemipelagites and turbidites, up to 2 km thick, and Pleistocene basin and alluvial sediments (Fig. 1; Fantoni and Franciosi, 2010 and references therein). This earthquake sequence has added strong hints to the definition of the active structures of this portion of the Northern Apennines external fronts. In fact, although with some differences, seismic, InSAR, GPS, and macroseismic data from the May–June 2012 sequence consistently suggest that two blind thrusts of the Ferrara arc activated during the 2012 mainshocks (Figs. 1 and 2), confirming the activity of the

external buried fronts (e.g. Burrato et al., 2003; Boccaletti and Martelli, 2004).

The seismic history of the past 30 yr (ISIDE Database, 2012; CSII.1, 2006) shows low seismicity in coincidence of the area hit by the 2012 sequence and the same appears true for the location of the main historical events (Rovida et al., 2011). In fact, apart from the VII–VIII MCS 1639 earthquake, based only on one data point in Finale Emilia, only earthquakes of moderate magnitude occurred in the area surrounding the 2012 seismic sequence (Fig. 2; Camassi et al., 2011; Castelli et al., 2012). The closest and more relevant is certainly the I = VIII MCS (M_w 5.5) 1570 earthquake that hit the area of Ferrara (Fig. 2), about 30 km east of the 2012 sequence. Historical accounts of the 1570 earthquake report occurrences of liquefaction phenomena in the area of Ferrara and surroundings as well as of open fractures and changes of the water flows in channels (Guidoboni et al., 2007). More recently, in 2011 a M_L 4.8 event hit the area about 20 km NE of the 2012 sequence (Fig. 2). Widespread secondary geological

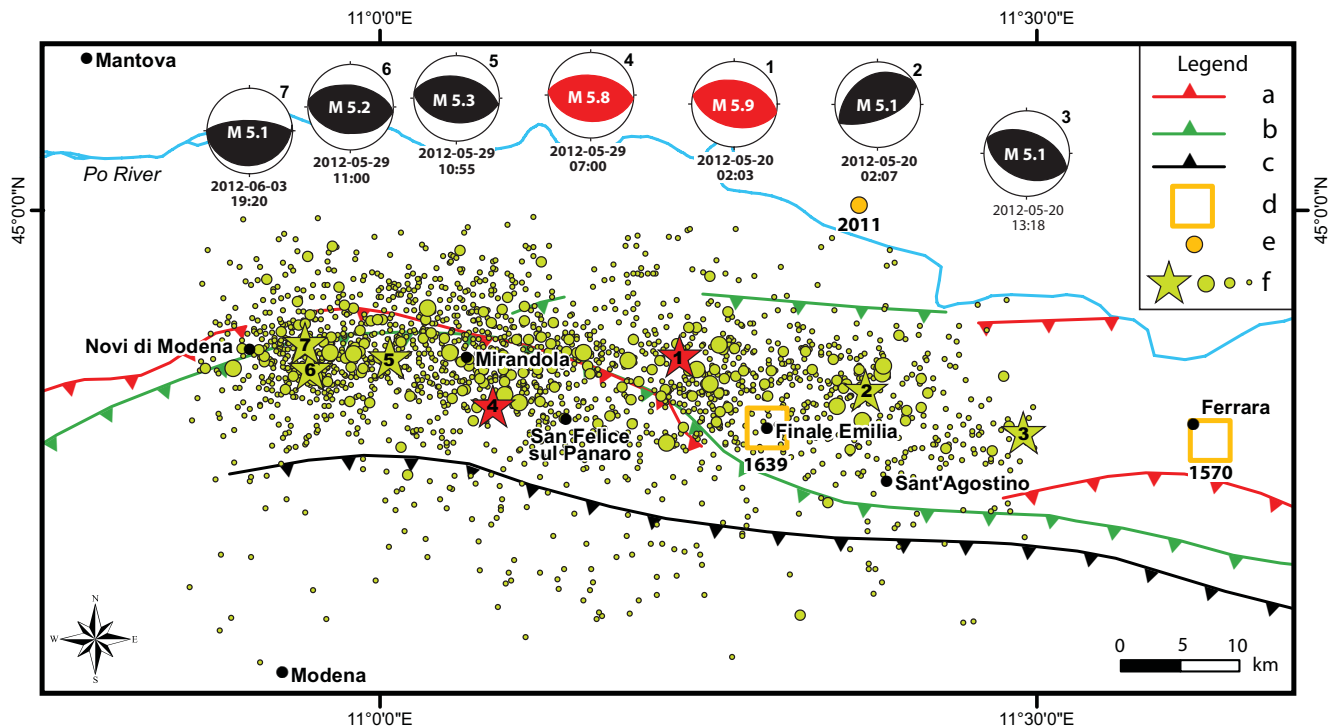


Fig. 2. Area of the Emilia 2012 earthquake sequence. (a), (b), (c) main active structures from Boccaletti and Martelli (2004), see caption of Fig. 1; (d) historical earthquakes with $M_e \geq 5$ (CPTI11 Catalogue, Rovida et al., 2011); (e) M_L 4.8, 2011 event and (f) Emilia 2012 sequence (ISIDe Database, 2012): stars stand for $M_L \geq 5.0$ earthquakes (in red the two mainshocks) and numbers refer to focal mechanisms (Scognamiglio et al., 2012); circles of variable size are for earthquakes of $M_L = 4.1 \div 4.9$, $M_L = 3.1 \div 4.0$ and $M_L \leq 3.0$.

effects were produced by the 2012 Emilia sequence and are mainly related to liquefaction phenomena. INGV-Emergeo Working Group, as well as teams from other institutions (e.g. ISPRA, University of Insubria, Emilia Romagna Geological Survey, etc.), promptly surveyed the area to collect coseismic geological evidence (for a complete photographic coverage see Emergeo Working Group, 2012b), coordinating and integrating information to assure the maximum coverage of the affected area. All the survey teams verified that no primary surface rupture occurred. In this paper we present the data collected by the Emergeo Working Group through the following approaches: (i) field survey; (ii) helicopter and powered hang-glider trike survey; (iii) reports from local people collected in the field or through a Web-based survey activated at the INGV portal <http://www.haisentitoilterremoto.it/emergeo.html> (did you see earthquake geological effects?). For an extended description of the methodologies and technologies used for the survey of the geological effects, see Emergeo Working Group (2012a).

The significance of the collected data as a key to a better understanding and evaluation of the liquefaction hazard is then discussed in light of the local geological and geomorphic setting, the coseismic displacement defined by InSAR interferograms, the seismic sequence and the damage distribution.

2 The observed liquefaction phenomena

The most common geological features observed during the post-earthquake survey were related to liquefaction process. Thanks to the information provided by several local eye-witnesses and also based on the magnitude and timing of the main events, we conclude that the liquefaction process was induced by the 20 and 29 May mainshocks. In fact, the only large aftershock that could have produced liquefaction that would have been indistinguishable to eye-witnesses is the 20 May 2012, M_L 5.1, event that occurred only 4 min after the first mainshock (Fig. 2). However, this possibility is ruled out because looking at the national and international empirical relationships (magnitude vs. liquefaction; e.g. Galli, 2000; Obermeier, 1996), there are very few cases of liquefaction induced by earthquakes with a magnitude below 5.5.

Liquefaction is a hydrological phenomenon that originates by significant shaking during earthquakes, mainly on alluvial and coastal plains. The strength and stiffness of saturated and unconsolidated fine sediment at shallow depth (max. 30 m b.g.s.) are reduced by being shaken to a critical level where the effective stress tapers to zero and the sediments become fluid-like, i.e. liquefy. In this process, the over-pressured interstitial water tends to escape upward through newly formed, pre-existing fractures and/or anthropic structures (e.g. water wells, foundations, etc.), conduits and vents

bringing along the liquefied sediment to the surface and forming sand volcanoes and sand sheets. Based on the above description, it is clear that the Po Plain, filled by alluvial sediments hosting multilayered confined aquifers and phreatic aquifers in the first 10 to 30 m (Regione Emilia Romagna, ENI-Agip, 1998; Marcaccio and Martinelli, 2012), has a high potential for liquefaction; this earthquake sequence has certainly confirmed it.

On the basis of their morphologic and structural characteristics, the observed coseismic effects at the surface were grouped into three main categories (Fig. 3); (i) liquefaction; (ii) fracture/liquefaction; and (iii) fracture. Categories (i) and (ii) may be associated to relevant but localised subsidence or bulging related to sediments extrusion. Under the liquefaction category we classified single spots such as sand volcanoes, scattered vents and coalescent flat cones, sand infilled water wells, fountains and manholes. The fracture/liquefaction category comprises mainly elongated and aligned multiple sand volcanoes, and sand flows from coseismic open fractures occurring both on natural and paved ground surface. Finally, the fracture category includes newly formed open fractures and cracks without evident sand extrusion at the surface. The surveyed features appear independent from the type of environment, in fact they occur on roads, buildings, backyards, parks, agricultural fields, etc. Some manmade underground structures such as wells, foundations, sewers, etc. forming artificial boundaries represent a simpler escape for the overpressured water.

Besides categorising attributions to specific typologies, we collected structural and morphological data of the observed geological surface effects. In particular we measured (1) thickness of the sand volcanoes and area of sand draping; (2) morphology and diameter of the sand outlets; (3) spacing of the sand outlets, length and strike of their alignments; (4) spacing, length and strike of the fractures and of the sand outlet alignments; (5) style of the fractures pattern; and (6) opening and offset of the fractures. Samples of the liquefied extruded sand were collected for sedimentological analysis. The aerial survey integrated the dataset collected in the field by the analysis of more than 1500 georeferenced photographs and of more than 3 h of video. The low-altitude flight plan (~200–300 m) contributed to cover the mesoseismal area, having the resolution necessary to detect the presence or the absence of surface coseismic geological effects. Most of the aerial observations were validated by field survey, or, when this was not possible, the careful analysis of the images allowed attribution of each feature to one category and measurement of at least length, strike, and areal extent. Considering the land use, typology and status of the cultivations covering the flat land, it is possible that some minor evidence was missed but only in coincidence of wheat fields. The georeferenced photographs were analysed and, jointly with the field data, the observations were stored, analysed and managed in a geographical information system.

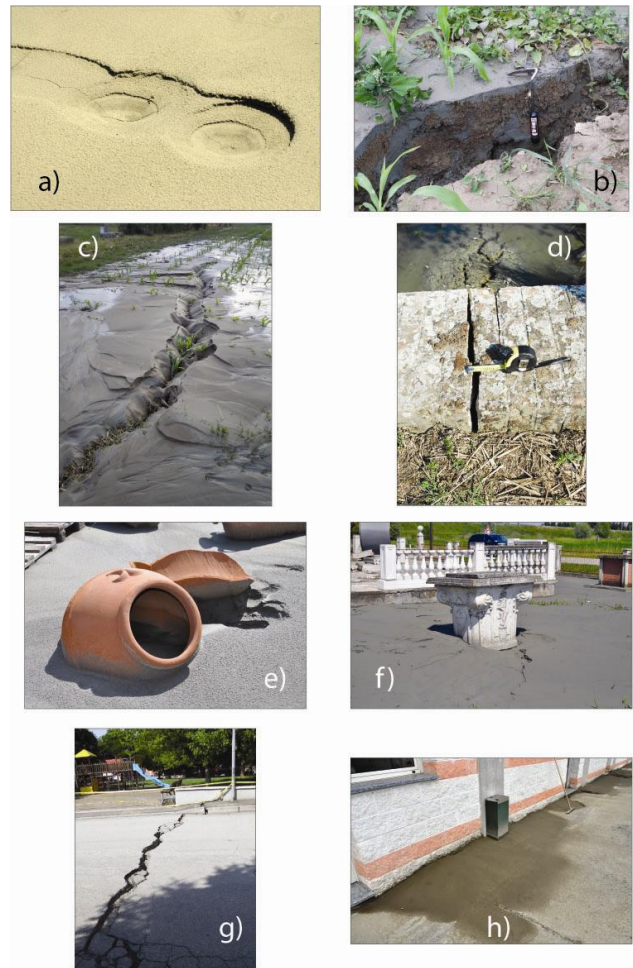


Fig. 3. Examples of surface phenomena produced by the 2012 Emilia sequence on the ground and on manmade structures: (a) detail of aligned multiple sand blows nearby Sant'Agostino; (b) ~20 cm-wide open fracture with liquefaction near San Carlo. It is possible to observe several cm-wide, grey sand-filled cracks that represent the path to the surface of the liquefied material; (c) 30 m-long open fracture with massive ejection of dark grey sand in San Carlo (photo by L. Ghidoni); (d) fracture affecting the bridge over a channel filled with liquefied sand near Burana; (e) the warehouse of this pottery shop in San Carlo was covered by a ~15 cm-thick layer of liquefied sands and silts; (f) liquefied sand filled this water well and poured out to cover a ~500 m² circular area; (g) fracture affecting a paved road in San Carlo; (h) the ground/building limit often represented a preferential way of outflow for liquefaction, like in this case at San Felice sul Panaro.

As a whole, a total of 1362 sites with geologic coseismic effects were identified and surveyed over more than 1200 km²; 768 findings were classified as fracture/liquefaction, 485 as liquefaction, and 109 as fracture.

As it appears clearly from Fig. 4, the coseismic effects are not evenly distributed over the area but mostly appear concentrated and aligned. For the whole mesoseismal area, the preferential trend of the linear features (fractures and

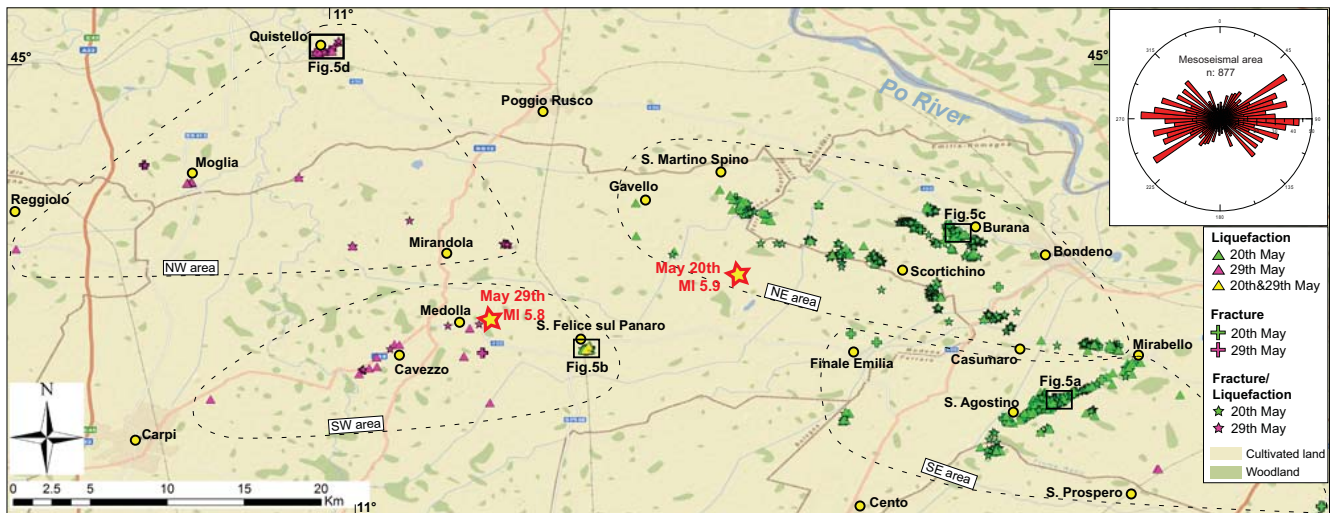


Fig. 4. Location of observed geological effects (1362 data points) distinguished according to the three main categories and the triggering seismic event. The two mainshocks and the four study areas are presented. The inset shows the rose diagram evidencing the trend distribution of the linear coseismic geological effects (877 fractures and fracture/liquefactions).

fracture/liquefactions) ranges between N060–N120. In the following, the collected data are presented by subdividing the surveyed region in four areas: SE, SW, NE, NW (Figs. 4 and 5). This is not only a geographic division but reflects also feature characteristics, such as (1) space distribution, (2) time of occurrence, (3) prevalent typology, and (4) distinctive arrangement patterns.

2.1 The SE area

Within the area comprising the villages of Mirabello, Sant'Agostino, San Prospero, Cento, and Finale Emilia, the observed coseismic features belong to all three categories: liquefaction, fracture/liquefaction, fracture. Over a total of 478 observations, 45 % were liquefactions, 40 % fracture/liquefactions, and 15 % fractures (Fig. 4). Most of these effects occurred during the 20 May shock. A peculiar high density of observations is located between Mirabello and Sant'Agostino villages. About 1/3 of the total number of observations in the whole area were collected here, in a NE–SW striking zone about 7 km-long and 0.2 to 0.6 km-wide. The interaction of liquefaction effects with man-made structures was particularly strong, especially in the village of San Carlo where many buildings, roads, fenced walls, and lifelines were severely affected and damaged by fracturing and liquefaction phenomena. Notably, a high percentage of the water wells in the area were filled by the liquefied sand, often up to the top.

The extruded sands (liquefaction and fracture/liquefaction category) were mainly grey medium-to-fine sand and in minor amount hazel sand, suggesting the liquefaction of at least two distinct sandy layers. In a few cases, the two sands were extruded at the same place, one following the other. The thickness of the extruded sand in open fields reached about

40 cm, whereas at sites in the San Carlo village garages or ground-floor apartments were filled with 1 m-thick sand bodies. Maximum observed diameter of sand volcanoes is 10 m that, when coalescing, extend to a maximum length of 50 m. Many fractures, mostly NE–SW striking, were associated with the extrusion of liquefied sand (fracture/liquefaction category), and many of them extended to a maximum length of 50 m, often showing up to 20 cm opening and more rarely 20 cm of vertical separation. The fractures with no sand extrusion had a similar strike, were up to a few hundred-m long, displayed usually a clear opening up to 30 cm, and locally showed a vertical separation up to 20 cm with both SE and NW downthrown (Fig. 5a). In some artificial cuts open to repair coseismically broken pipes, we observed open fractures infilled by grey sand that did not reach the surface. This is a further indication that the driving phenomenon here is related to liquefaction even if sand at some locations was not extruded and only fractures or soil bulges were observed. The large amount of extruded sand in the San Carlo area produced important emptying and compaction in the liquefied beds that produced at the surface a localised subsidence, sometimes accompanied by ponding. Subsidence started with the occurrence of liquefactions but, because settling and re-compaction of sediments is a slow process, it kept increasing day by day, representing a further hazard for the involved man-made structures. To understand this process, we started a terrestrial LiDAR (TLS) monitoring of the fractures and fracture/liquefactions crossing the Sant'Agostino-San Carlo cemetery. On 23 May, the amount of opening and vertical separation across the most prominent fracture visible in the northern wall of the cemetery was 10 cm and 3 cm down to SE, respectively.

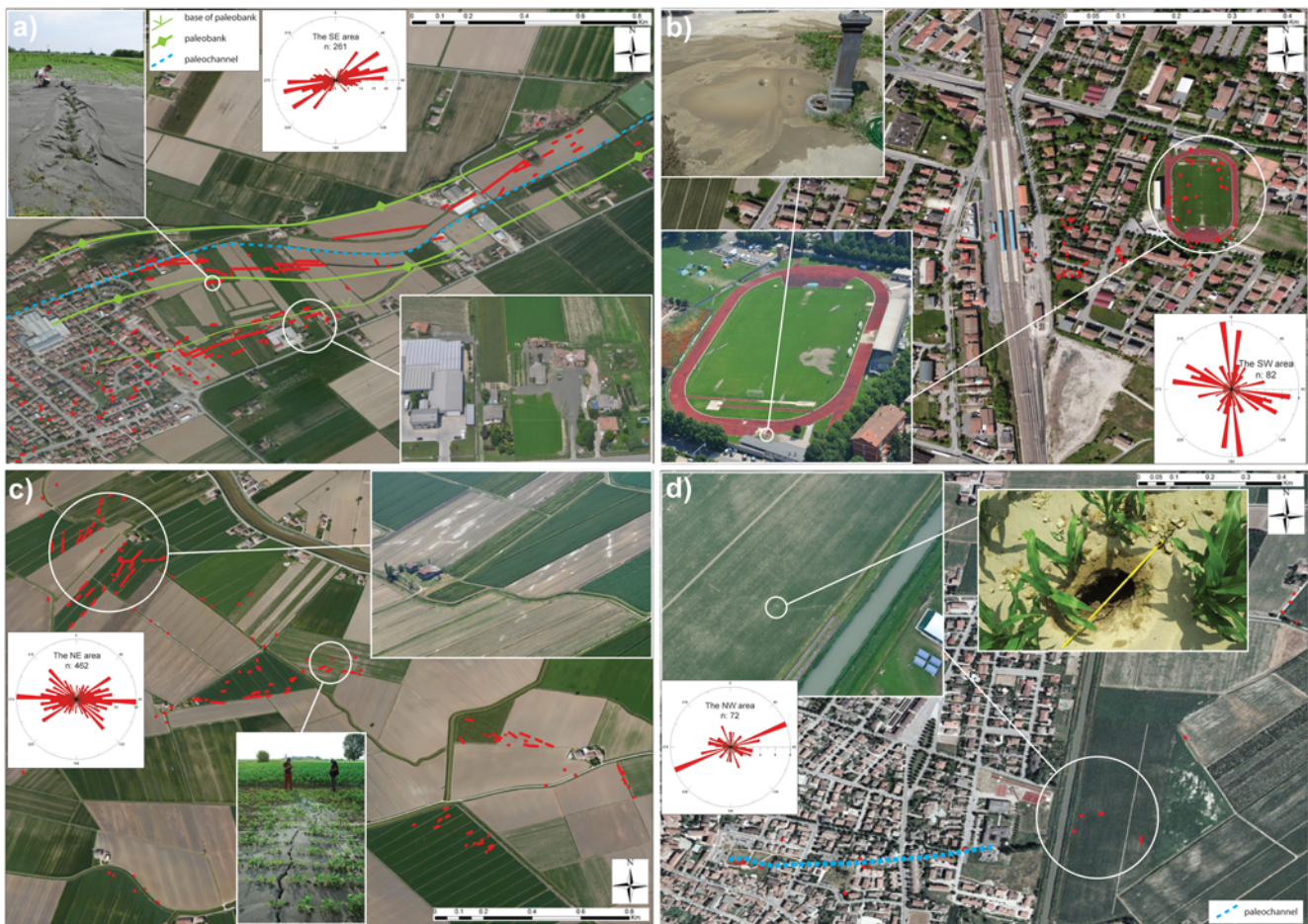


Fig. 5. Examples of coseismic geological effects of the four study areas at different scales of observation (satellite view from Bing Maps; aerial and field view from Emergeo survey). Red dots indicate the coseismic feature locations. The inset shows the rose diagram displaying the trend distribution of the linear coseismic geological effects. **(a)** SE area. Fractures and fractures/liquefactions following the paleochannel morphologies close to San Carlo village. The aerial view shows a large volume of sand outflow. The detail shows the fracture/liquefaction affecting the top of the paleobank; **(b)** SW area. Distribution of liquefactions and fractures/liquefactions at San Felice sul Panaro village. The aerial view shows the trends of the fractures/liquefactions affecting the soccer field. The detail shows the reactivation of the liquefaction occurred on 29 May through a water well; **(c)** NE area. Fractures/liquefactions showing a meander-like, complex alignment west of Bondeno village. The aerial view displays the variability of the fractures/liquefactions trends evidenced by the ploughed field. A detail of the fracture/liquefaction is shown; **(d)** NW area. Distribution of liquefactions and fractures/liquefactions at Quistello village aligned along a buried channel. The aerial view shows a ten-of-metres long fractures/liquefactions. A detail of the fracture/liquefaction presents a sink-hole with soil chips ejected over the sand volcano body.

On 31 May, the analysis of TLS data acquired on the south cemetery boundary wall allowed the estimation of a relative displacement along the direction normal to the wall of about 5 cm down to SE (total amount). It is noteworthy that the TLS data precision (for ranging scanner) is about 5–6 mm and the availability of high density coordinate point cloud achieved better values.

The method used to obtain morphological information from TLS analysis is based on the definition of reference planes (or other primitives) and on the computation of point-to-plane differences, allowing the creation of detailed maps (Fig. 6a; Pesci et al., 2011). The cemetery's surrounding

street was monitored, showing interesting features by means of TLS and GPS integration. In particular, three rapid static surveys (Pesci et al., 2012) were performed from 31 May to 12 June 2012. The results describe the terrain lowering with values ranging from 0.5 cm to about 2.0 cm along the street, showing differential movements (Fig. 6b) with a mean error of about 6–8 mm (2σ).

Other liquefaction related features were observed in this region but disconnected from the main Sant'Agostino-Mirabello zone. These were concentrated in two spots located at about 7 km westward and about 2 km southward of Sant'Agostino village. It is noteworthy that at Finale Emilia

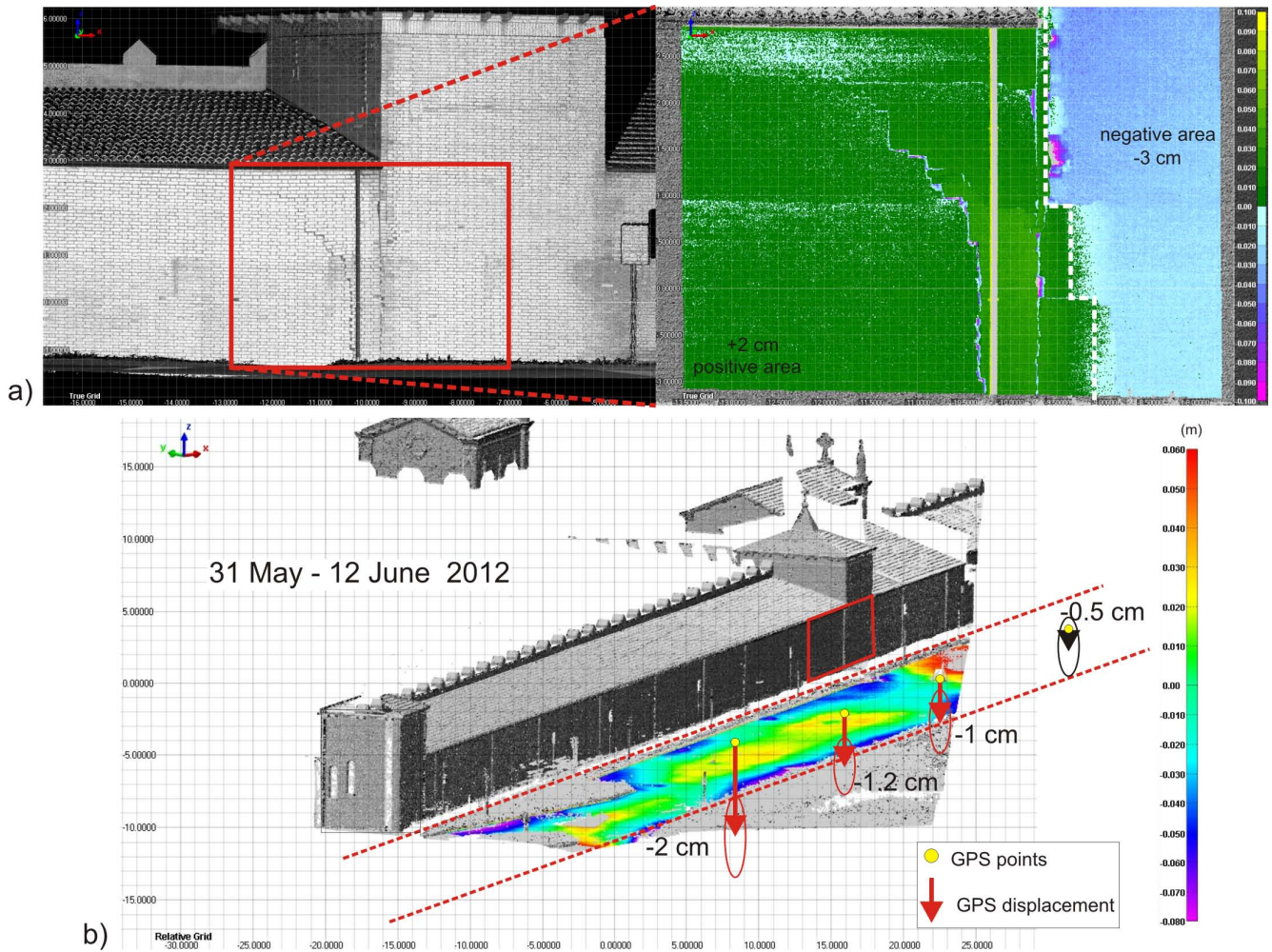


Fig. 6. (a) San Carlo cemetery wall deformation map across the fracture obtained through terrestrial laser scanning (TLS); (b) San Carlo cemetery surrounding street monitored by means of TLS and GPS integration, surveyed from 31 May to 12 June 2012 (terrain lowering: GPS measurements).

village and its surroundings, only minor fracturing occurred on a few paved roads and with no evidence of sand extrusions.

The preferential trend of the main subset of geological observations from Sant'Agostino and Mirabello ranges between 50° – 90° N (Fig. 5a).

2.2 The SW area

Within the area comprising the villages of San Felice sul Panaro, Cavezzo, Medolla, with over a total of 132 observations, 38 % were assigned to liquefaction, 53 % to fracture/liquefaction, and 9 % to fracture (Fig. 4). In some sites of this area the coseismic effects occurred following both the 20 and 29 May mainshocks. As in the SE area, here the extruded sands were mainly grey medium-to-fine sand and in minor amount hazel sand. The density of effects in this area were quite low; however, there were a peculiar high density

of observations collected at San Felice sul Panaro (produced by both 20 and 29 May shocks, Fig. 5b), where more than 100 liquefactions and fracture/liquefactions were mapped in a 0.2 km^2 area between the stadium and the railway station. Here, several water wells and manholes as well as ground–foundation boundaries served as artificial vents and are now completely filled by liquefied sand.

Another area with a relative concentration of effects (produced by the 29 May shock) is in the Cavezzo village, where liquefactions occurred prevalently within and near the main canal, and a few fracture/liquefactions were organised in a NE–SW striking zone about 3 km long and up to 0.7 km wide. Very few additional isolated coseismic features of liquefactions and fractures were mapped around the Medolla village.

In the SW area, linear features indicate two preferential trends: N–S and N100–N125 (Fig. 5b).

2.3 The NE area

This is another area with important concentration of geological coseismic effects produced by the 20 May mainshock (Fig. 4). In particular, in over a total of 636 observations, 27% were liquefactions, 70% fracture/liquefactions, and 3% fractures. All the identified liquefactions and fractures/liquefactions involved grey coarse-to-fine sands, not showing any significant difference as for their lithological characteristics and content at a glance. The geological features in the area appeared organised into two main WNW–ESE trending sets: a northern set comprised between the villages of Bondeno and San Martino Spino, and a southern set between Mirabello and Gavello (Figs. 4 and 5c).

The northern set comprised a high concentration of observations, west of the Bondeno and south of the Burana villages, mainly consisting in fractures/liquefactions and rare liquefactions. Fractures with sand extrusion were up to 20 m long, up to 10 cm wide, and thickness of the sand was up to 30 cm. Although they were sub-clustered in few tens-of-metres wide and some hundred-of-metres long strands, these features form a zone up to 1.5 km wide and about 4 km long. The zone mainly crosses agricultural fields and only one building was deeply affected by open cracks just south of Burana.

The southern set of effects comprises all the defined typologies although fracture/liquefaction features prevailed with lengths up to 50 m. Fractures/liquefactions and fractures were seen in a narrow (about 500 m wide) zone, just west of Mirabello, for a length of about 2 km. They were generally N110 to N140 trending, and about 100 m long (the longest in the area) (Fig. 5c). Fractures/liquefaction occurred also a few km north of Casumaro. Here, these were up to 100 m long, with a prevailing N130–N150 trend, and were comprised in a 500 m wide zone. Fracture/liquefactions were particularly concentrated in the area of Scortichino where they formed an up to 1 km wide zone, but comprising two clusters: one just E–SE of Scortichino, and another located few kilometres to the NW. The first cluster was characterised by N050 and N090 trends and rare N140–N160 oriented features; the second cluster had rather sparse directions and a maximum length of about 30 m. The presence of liquefaction-related features decreased rapidly to the W and NW of the area, where a few liquefactions and fractures/liquefactions were observed just E and SE of Gavello and S of San Martino Spino.

The main trend of the features in the NE area ranged between N060 and N140, with a maximum concentration in the E–W direction (Fig. 5c).

2.4 The NW area

The survey of this area started in detail following the 29 May mainshock (Fig. 4) because only limited effects were reported after the 20 May seismic event. Field and aerial sur-

veys revealed a low density of coseismic effects with mainly sparse and scattered evidences. In over a total of 116 mapped effects, 38% were liquefactions, 59% fracture/liquefactions, and only 3% fractures (Fig. 4). The extruded sediment, both by vents or fractures, was consistently made by grey fine sand all over the area. The amount of out-flown sand in individual sand blows rarely draped a ground floor exceeding 10 m² and the vents did not build sand volcano bodies taller than 30–35 cm. Concerning the coseismic fractures, the ground failure consisted in open cracks with lateral separation of maximum 30 cm, with no vertical sizable offset. In only one case a sink-hole, 50 cm wide and 50 cm deep, in coincidence of liquefaction outlet, was observed, presenting evidence of soil chips ejected over the sand volcano body up to a distance of 1.5 m (Fig. 5d).

Most of the surface effects were localised close to the Moglia and Quistello villages. The latter presented the largest amount of fractures accompanied by liquefactions, which appeared to be organised in a system of metres-long segments striking from N060 to N120 that describe a WSW–ENE oriented, ~400 m long alignment. By tracking single liquefaction outflows and subordinate fractures with liquefactions apparently controlled by anthropic structures (i.e. water wells, building foundations, sewage systems, etc.), this alignment appeared to extend 600 m further west into the urban area. Inside the Moglia village, ~20 sand blows of grey fine sand, whose outlets appeared facilitated by the presence of buried anthropic structures, described an E–W strip of ~300 m. Another relevant coseismic effect occurred 2.0 km west of the Moglia village, where an E–W striking, 50 m long, 30 cm open fracture was accompanied by alignment of liquefaction outlets and sand draping of ~500 m².

In the remaining area, single fracture/liquefaction and liquefaction features were detected at places with the standard expression observed elsewhere, with small size and no clear indication of structural arrangement.

The main trend of the features in this area was about N070 (Fig. 5d).

3 Discussion

Extensive liquefaction was observed following the two mainshocks of the 2012 Emilia seismic sequence in an area of more than 1200 km² within the alluvial Po Plain. Liquefaction is a typical secondary coseismic effect that often affects alluvial and coastal plains, as recently occurred in both the 2010 and 2011 Darfield/Christchurch earthquakes in New Zealand, and the 2011 Tohoku earthquake in Japan.

Figure 4 clearly shows that the sites of liquefaction produced by the 2012 Emilia earthquakes are localised in both clusters and alignments. This is an indication that, although the morphology of the activated area appears homogeneously flat with very small differences in elevation and quite monotonous from a geologic point of view, there should

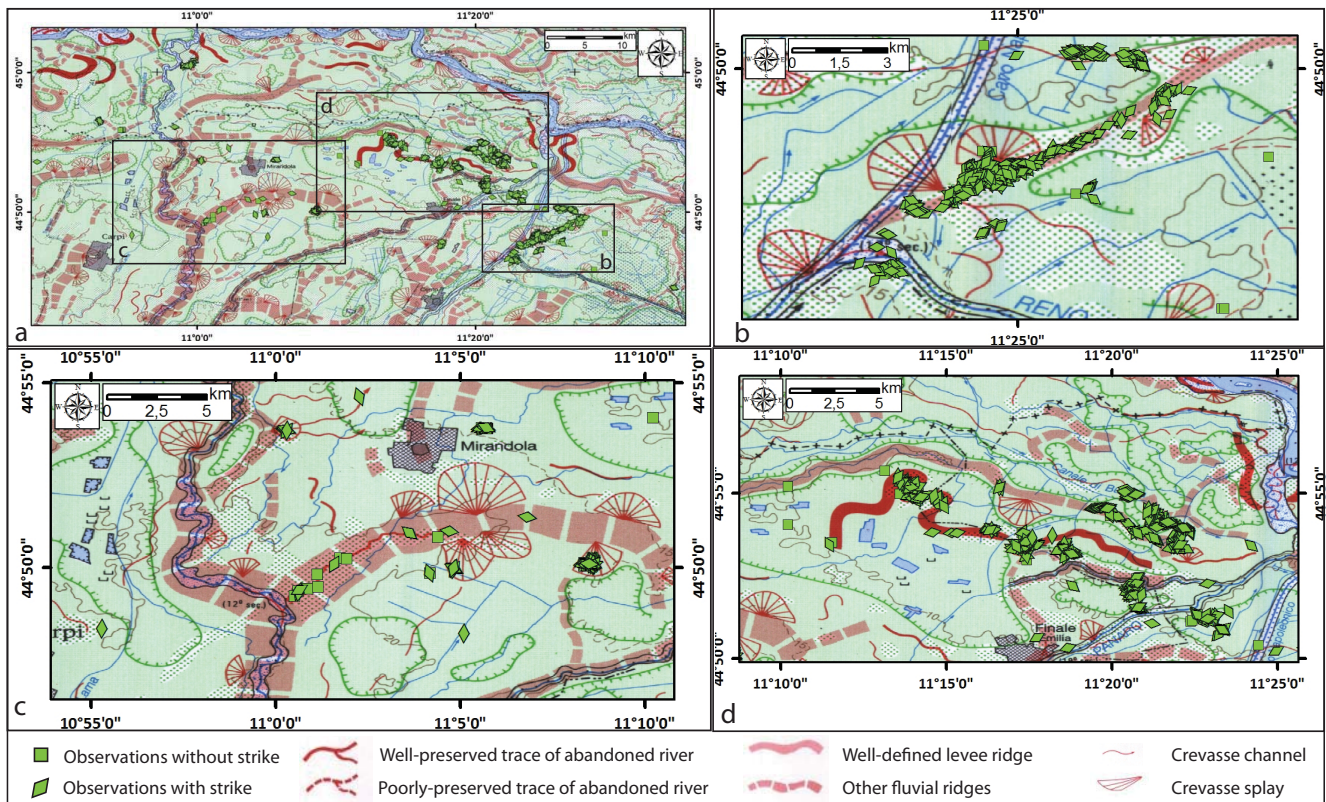


Fig. 7. (a) Comparison between the geomorphic characteristics of the area (Castiglioni et al., 1999) and the location of the observed geological effects. (b), (c) and (d) Details of the SE, SW and NE areas, respectively.

be a local characteristic that increases the susceptibility of sediments to liquefaction.

A first comparison between the geomorphic characteristics of the area (Castiglioni et al., 1999) and the location of liquefaction and fracturing sites shows a good correlation of liquefaction with the location of the paleo-river channels, outflow channels, and fans of the Secchia, Panaro and Reno rivers and with the levees of the Cavo Napoleonico channel (artificial channel, connecting the Reno and Po rivers, initiated in 1807). Due to their origin, most of these features are slightly higher (1–2 m) in elevation with respect to the basal level of the plain. Further support of this correlation is that the prevailing liquefaction alignments and fracture systems (with or without liquefactions) follow the main direction of the paleo-riverbeds (Fig. 7).

Stratigraphy of the upper 10–20 m of cores existing in the area (available at the Emilia Romagna Website, <http://ambiente.regione.emilia-romagna.it/geologia/cartografia/webgis-banchedati/sezioni-geologiche-prove-geognostiche-pianura>) highlights that, in proximity of the paleo-riverbeds, the upper 5–7 m contain several layers of fine sand that commonly host surficial aquifers (Marcaccio and Martinelli, 2012) and below them there are only finer sediments. Conversely, far from paleo-riverbeds, the upper stratigraphy is mainly

composed by silt and clay not hosting aquifers. This is a further suggestion that liquefaction occurred in the saturated sandy layers of the upper 5–6 m that likely characterise paleo-riverbeds, outflow channels, fans, and levees. The vertical and lateral heteropic changes in the stratigraphy, as those occurring in alluvial plains, strongly control the location of liquefaction as was already observed during the 1811–1812, New Madrid (central USA), earthquake sequence (Tuttle, 2001). There, liquefaction sites appear aligned along the river bar deposits that may have contacts and stratigraphy that favoured the escape of slurries of sand and water toward the surface.

Further understanding of the significance of the coseismic geologic data can be derived from a comparison with the ground deformation field measured by InSAR (Pezzo et al., 2013; Bignami et al., 2012; Salvi et al., 2012). The co-seismic SAR interferograms available for the Emilia sequence are shown in Fig. 8. The Radarsat interferogram (Fig. 8a) represents the cumulative deformation relative to the largest shocks and shows a large scale fringe pattern characterised by an average E–W trend of the deformation, with two well-defined uplift lobes (with slightly different orientations) parallel to the activated faults. The COSMO-SkyMed interferogram in Fig. 8b covers only the easternmost part of the displacement field of the 20 May mainshock and shows a

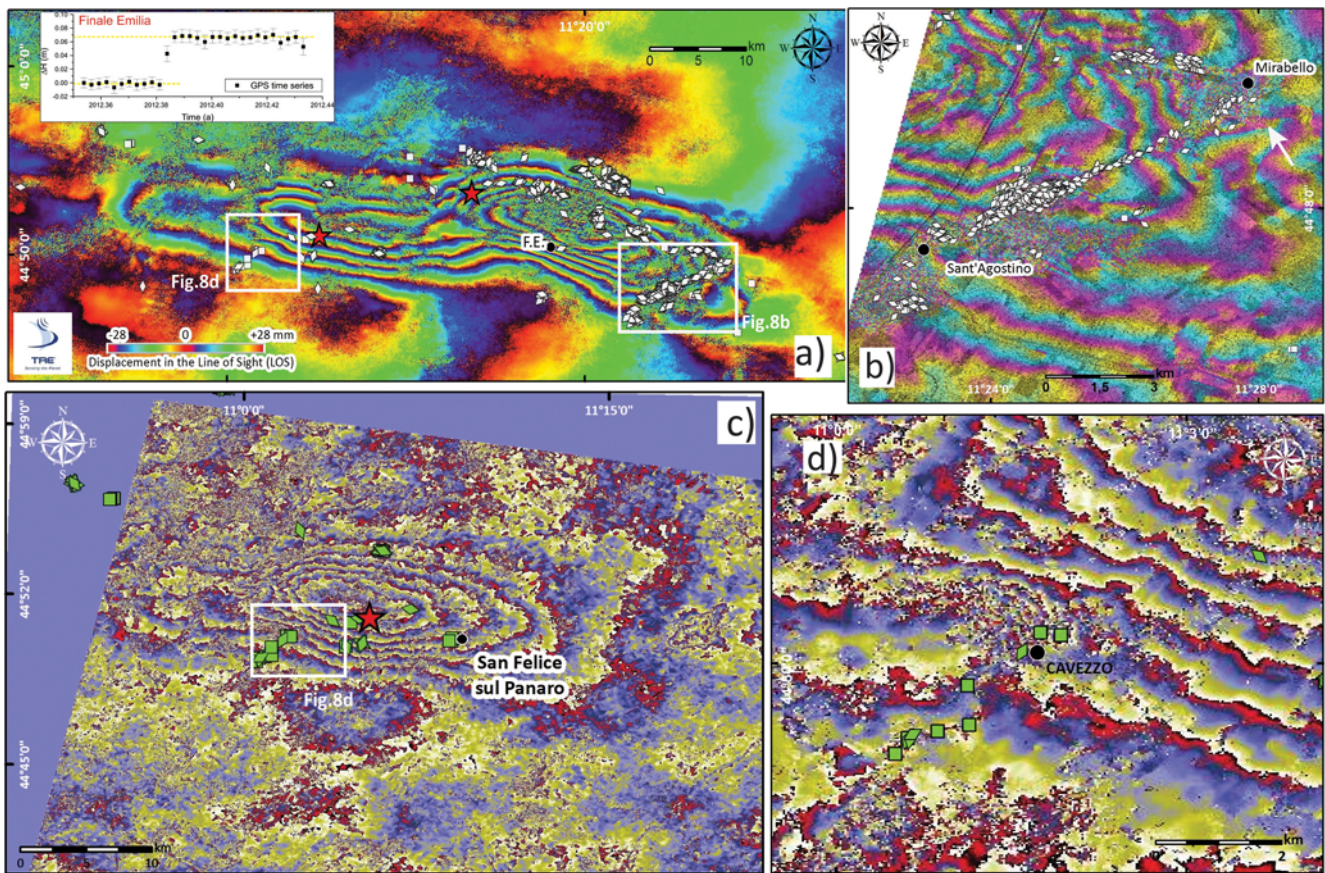


Fig. 8. Interferograms showing the coseismic deformation field and the local coseismic effects observed at surface. The site effects are marked with diamonds whose major axis parallels the feature strike, and with squares if no strike data are available. **(a)** Radarsat interferogram processed by the T.R.E. company (modified from www.treuropa.com). It represents the cumulative deformation relative to the largest mainshocks (time window: 12 May–5 June). The inset shows the data from continuous GPS station located at Finale Emilia indicating a clear coseismic height variation of about 6.5 cm on 20 May (Baldi et al., 2009); **(b)** COSMO SkyMed image showing the easternmost deformation field of the 20 May mainshock (red star). White arrow points to the abrupt deviations of the fringes strike; **(c)** COSMO SkyMed image of the full deformation field of the 29 May mainshock (red star). Diamonds and squares symbols locate the effects observed following the 29 May event (newly formed and/or reactivation of 20 May features); **(d)** enlargement of the southwest portion of interferogram in **(c)**. All COSMO interferograms were processed by the Sigris Project (Pezzo et al., 2013).

concentric fringe pattern with a maximum uplift of ~ 15 cm, occurring about 7 km east of Finale Emilia (upper left side of the image). Another COSMO interferogram (Fig. 8c) shows the whole deformation field relative to the 29 May event. For this event, the maximum ground uplift was 12 cm, located close to the Mirandola village.

An initial interesting observation is that most of the data collected at the surface (white diamonds and squares in Fig. 8a) are enclosed within the area of significant deformation measured by InSAR and coincide also to the area of aftershocks concentration (Fig. 9). The observed ground features were mainly clustered at the borders of the deformed area, while a very few number of effects occurred in the area of maximum uplift (Fig. 8a) because, there, no paleo-riverbeds exist (Fig. 7). This lack of stream beds is the result of the long-term growth of the local buried geologi-

cal structures (e.g., Burrato et al., 2012) through repeated earthquakes similar to the 2012 one. The accumulation of repeated deformation tends to produce the diversion of the stream beds from the elevated areas (where repeated maximum coseismic uplift occurred) toward the lowlands. The high resolution of the COSMO SkyMed images allows drawing additional inferences on the spatial distribution of the local geological effects at surface. In particular, the alignments of severe liquefactions and fractures coincide with small scale and well-defined areas of SAR signal decorrelation. Near the decorrelated areas, sharp deviations of the fringe strike from the large scale trend occur, with amplitudes varying from hundreds up to thousands of metres (Fig. 8b). The locations of such peculiar fringe patterns often coincide with the mapped paleo-riverbeds (Fig. 7) as between the villages of Mirabello and Sant'Agostino, where there is also a

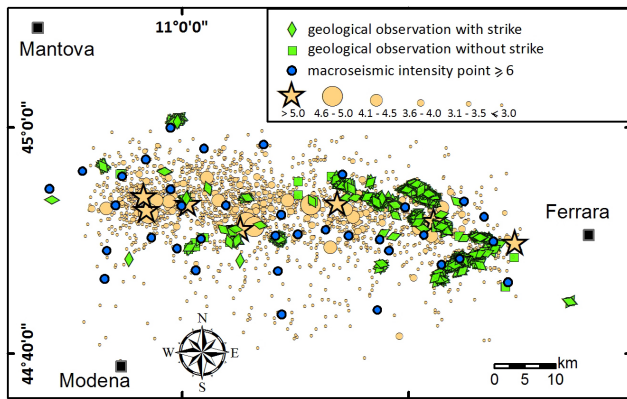


Fig. 9. Map of intensity ≥ 6 EMS of the 2012 Emilia sequence (blue circles, modified from Tertulliani et al., 2012), compared with the epicentres (yellow circles) and with the liquefaction pattern (green diamonds and squares).

prominent NE–SW alignment of surface coseismic features (SE area, see Sect. 2.1; Fig. 8b). This alignment compares very well to an area of SAR signal decorrelation, whose origin is likely due to co-seismic modifications of the surface scattering properties caused by the expulsion of ground waters as already observed by Atzori et al. (2012) for the 2011 Christchurch earthquake in New Zealand. Along and close to the eastern section of this alignment, complex ground deformations occur, indicated by sharp bending (up to 90°) of the local fringe trends (white arrow in Fig. 8b). These latter features indicate areas of differential subsidence characterised by cross dimensions (up to 3 km) significantly larger than the alignment of the liquefaction effects. Such phenomena are possibly related to differential compaction or fluid migration due to the presence of significant lateral heterogeneities in the sedimentary bodies forming the ancient riverbeds. The close-up in Fig. 8c shows the area of the Cavezzo village (SW area, see Sect. 2.2), another site where the coincidence between liquefaction features, decorrelation in the SAR signal and fringe pattern “disturbances” were identified.

Another aspect to be discussed on the basis of the collected liquefaction data is about their distribution with respect to the location of the causative earthquake, which is relevant for the definition of the liquefaction hazard. The Emilia earthquake sequence affected an open and wide alluvial valley with a quite homogeneous geomorphic setting. The survey of the liquefaction sites can be considered complete as it was systematically performed with different approaches and was verified with the findings of other groups of surveyors (among them, ISPRA, 2012; Uni Insubria, 2012; Regione Emilia-Romagna, 2012); also, the location, size and source characteristics of the causative earthquakes are known (e.g. Bignami et al., 2012). The Emilia 2012 liquefaction dataset is thus an exceptional case study, especially if compared to the handful of related observations from contemporary reports on the past ~ 1000 yr, of earthquakes whose

location and size contain relevant uncertainties, and mainly from areas with complex geomorphology (e.g. narrow and small intramountain valleys in the Apennines). Empirical relations, both global (Obermeier, 1996) and regional (Galli, 2000), show that the occurrence of liquefaction depends on the earthquake magnitude and on the distance from the epicentre, suggesting a maximum distance of 30–40 km for the occurrence of liquefaction in cases of a $M \sim 6$ earthquake. The furthest observed liquefaction from the 2012 epicentres is located at about 30 km (only one site at 40 km), for the 20 and 29 May earthquakes. However, it is interesting to note that the distribution area of liquefaction mimics the E–W elongated area of the aftershocks and that of surface deformation depicted by the InSAR. This supports the observation that the spatial distribution of liquefactions is within the expected distances with respect to the mainshocks but displays a pattern related to the earthquake source geometry (e.g. Tuttle, 2001). In this case, the E–W liquefaction distribution elongated pattern is probably more prominent because of the combined occurrence of the two events aligned in an E–W direction. However, considering that the manifestation of liquefaction is related to the largest ground accelerations that, at their turn, depend on the source geometry and on rupture kinematics, the elongated distribution of geological effects may provide insights into the understanding of the source geometry and of the damage area. It is interesting to note that, by plotting the damage distribution from Tertulliani et al. (2012), the highest intensities distribution ($I \geq 6$ EMS) coincides with the liquefaction area (Fig. 9), confirming that, similarly to damage, the liquefaction distribution (although is a secondary geological coseismic effect) has a direct relation to the earthquake source characteristics, at least for similar-sized earthquakes.

All this highlights the potential for the use of paleo-liquefactions observations to investigate the related earthquake source and the possibility of a reconsideration of historical and paleo-liquefaction distributions to better understand the characteristics of the earthquake source (e.g., De Martini et al., 2012; Tuttle, 2001; Tuttle et al., 2002).

4 Conclusions

The 2012 Emilia seismic sequence hit a wide area of the southern Po Plain. Because of its high susceptibility to liquefaction of the alluvial plain, this seismic sequence produced the most prominent extensive liquefaction phenomena of the last century in Italy (Figs. 3, 4 and 5). The Emergeo Working Group performed a systematic survey of the earthquake sequence area through field, aerial and interview approaches. A total of 1362 observation points were collected, stored in a geographical information system, and made partially available at the address <http://www.esriitalia.it/emergeo/>. The observations were grouped into three categories: (i) liquefaction; (ii) fracture/liquefaction; and (iii) fracture. The

distribution of liquefaction effects over the territory is uneven and appears mostly controlled by the presence of paleo-riverbeds, levees, out-flow channels and fans (Fig. 7) that are characterised by the presence of sandy layers in the upper 5 m. The maximum distance of observed liquefaction from the related earthquake epicentre is 30 km, in agreement with the regional empirical relations proposed by Galli (2000). Noteworthy, the envelope of all the liquefaction observations is not a circle around the causative earthquake epicentre but has an elongated shape mimicking the aftershock area, the InSAR deformation area and the $I \geq 6$ (EMS) area. In terms of liquefaction hazard evaluation, the liquefaction distribution reflects the combined effects of the low resistance of the soil to liquefaction (loose cohesionless soil with high water table) and the intensity of the ground motions that can be related in first approximation to the earthquake source characteristics (e.g. Tuttle, 2001). The broad area of occurrence of liquefaction can be roughly represented as the projection to the surface of the seismogenic source (or as the area of surface deformation); within this area, the stratigraphy and hydrological conditions of the upper 5–10 m are a further discriminator and better defines the areas prone to liquefaction. Future systematic coring and correlation with the extruded sands will allow the definition and characterisation of the sandy layers that liquefied (at least two different layers according to the collected observations). This information can be very useful to trace, also outside the current earthquake area, the zones with high potential for liquefaction. To conclude, it is worth remarking that careful geological and geomorphic investigations, integrated to the knowledge of the active faults with seismic potential, can provide the basis for a realistic evaluation of the potential for liquefaction in alluvial and coastal plains. Considering that plains are the most common areas for human developments and infrastructures, this is a topic of high societal impact.

Acknowledgements. We are indebted to the Corpo Forestale dello Stato for allowing us two helicopter surveys, the Municipalities, Carabinieri and Fire brigades for their technical support and especially all the people who contributed directly to the survey in the field or through the Web. A special thanks to L. Ghidoni, G. Bocchi, L. Larsen, O. Gallerani, L. Mazza, M. Bertazzoni and M. Borgonuovo for sharing with us their photographs. ASI and DPC provided the COSMO-SkyMed images. We thank R. Giuliani, L. Candela, S. Zoffoli and A. Coletta for their support and M. Lanzarini for the powered hang-glider trike survey. We are grateful also to P. Guarnieri and to an anonymous reviewer who, with their comments and suggestions, helped improve the paper. The Radarsat interferogram is copyright of TeleRilevamento Europa srl, Milan.

Edited by: O. Katz

Reviewed by: P. Guarnieri and one anonymous referee

References

- Atzori, S., Tolomei, C., Antonioli, A., Merryman Boncori, J. P., Bannister, S., Trasatti, E., Pasquali, P., and Salvi, S.: The 2010–2011 Canterbury, New Zealand, seismic sequence: multiple source analysis from InSAR data, and modeling, *J. Geophys. Res.*, 117, B08305, doi:10.1029/2012JB009178, 2012.
- Baldi, P., Casula, B., Cenni, N., Loddo, F., and Pesci, A.: GPS-based monitoring of land subsidence in the Po Plain (Northern Italy), *Earth Planet. Sc. Lett.*, 288, 204–212, 2009.
- Bignami, C., Burrato, P., Cannelli, V., Chini, M., Falcucci, E., Ferretti, A., Gori, S., Kyriakopoulos, C., Melini, D., Moro, M., Novali, F., Saroli, M., Stramondo, S., Valensise, G., and Vannoli, P.: Coseismic deformation pattern of the Emilia 2012 seismic sequence imaged by Radarsat-1 interferometry, *Ann. Geophys.*, 55, 789–795, doi:10.4401/ag-6157, 2012.
- Boccaletti, M. and Martelli, L. (Coords): Carta sismo-tettonica della Regione Emilia-Romagna scala 1 : 250.000 e note illustrative, Selca, Firenze, 2004.
- Burrato, P., Ciucci, F., and Valensise, G.: An inventory of river anomalies in the Po Plain, Northern Italy: evidence for active blind thrust faulting, *Ann. Geophys.*, 46, 865–882, doi:10.4401/ag-3459, 2003.
- Burrato, P., Vannoli, P., Fracassi, U., Basili, R., and Valensise, G.: Is blind faulting truly invisible? Tectonic-controlled drainage evolution in the epicentral area of the May 2012, Emilia-Romagna earthquake sequence (northern Italy), *Ann. Geophys.*, 55, 525–531, doi:10.4401/ag-6182, 2012.
- Camassi, R., Castelli, V., Molin, D., Bernardini, F., Caracciolo, C. H., Ercolani, E., and Postpischl, L.: Materiali per un catalogo dei terremoti italiani: eventi sconosciuti, rivalutati o riscoperti, *Quaderni di Geofisica*, 96, 51 pp., available at: <http://istituto.ingv.it/1-ingv/produzione-scientifica/quaderni-di-geofisica>, 2011.
- Castelli, V., Bernardini, F., Camassi, R., Caracciolo, C. H., Ercolani, E., and Postpischl, L.: Looking for missing earthquake traces in the Ferrara-Modena plain: an update on historical seismicity, *Ann. Geophys.*, 55, 519–524, doi:10.4401/ag-6110, 2012.
- Castiglioni, G. B., Biancotti, A., Bondesan, M., Cortemiglia, G. C., Elmi, C., Favero, V., Gasperi, G., Marchetti, G., Orombelli, G., Pellegrini, G. B., and Tellini, C.: Geomorphologic map of the Po Plain, Italy, at a scale of 1:250000, *Earth Surf. Proc. Land.*, 24, 1115–1120, doi:10.1002/(SICI)1096-9837(199911)24:12<1115::AID-ESP38>3.0.CO;2-Z, 1999.
- CSII.1: Italian Seismicity Catalogue 1981–2002, version 1.1., INGV-CNT, <http://csi.rm.ingv.it/>, 2006.
- De Martini, P. M., Cinti, F. R., Cucci, L., Smedile, A., Pinzi, S., Brunori, C. A., and Molisso, F.: Sand volcanoes induced by the April 6th 2009 Mw 6.3 L'Aquila earthquake: a case study from the Fossa area, *Italian Journal of Geosciences*, 131, 410–422, doi:10.3301/IJG.2012.14, 2012.
- Devoti, R., Esposito, A., Pietrantonio, G., Pisani, A. R., and Riguzzi, F.: Evidence of large scale deformation patterns from GPS data in the Italian subduction boundary, *Earth Planet. Sc. Lett.*, 311, 230–241, doi:10.1016/j.epsl.2011.09.034, 2011.
- Emergeo Working Group: Alessio, G., Alfonsi, L., Brunori, C. A., Burrato, P., Casula, G., Cinti, F. R., Civico, R., Colini, L., Cucci, L., De Martini, P. M., Falcucci, E., Galadini, F., Gaudiosi, G., Gori, S., Mariucci, M. T., Montone, P., Moro, M., Nappi, R., Nardi, A., Nave, R., Pantosti, D., Patera, A., Pesci, A., Pignone, M., Pinzi, S., Pucci, S., Vannoli, P., Venuti, A., and Villani, F.:

- Technologies and new approaches used by the INGV EMER-GEO Working Group for real time data sourcing and processing during the Emilia Romagna (Northern Italy) 2012 earthquake sequence, *Ann. Geophys.*, 55, 689–695, 2012; doi:10.4401/ag-6117, 2012a.
- Emergeo Working Group: Alessio, G., Alfonsi, L., Brunori, C. A., Burrato, P., Casula, G., Cinti, F. R., Civico, R., Colini, L., Cucci, L., De Martini, P. M., Falcucci, E., Galadini, F., Gaudiosi, G., Gori, S., Mariucci, M.T., Montone, P., Moro, M., Nappi, R., Nardi, A., Nave, R., Pantosti, D., Patera, A., Pesci, A., Pignone, M., Pinzi, S., Pucci, S., Vannoli, P., Venuti, A., and Villani, F.: A photographic dataset of the coseismic geological effects induced on the environment by the 2012 Emilia (northern Italy) earthquake sequence, on *Miscellanea INGV*, 16, ISSN 2039-6651, 2012b.
- Fantoni, R. and Franciosi, R.: Tectono-sedimentary setting of the Po Plain and Adriatic foreland, *Rend. Fis. Acc. Lincei*, 21, Supplement 1, S197–S209, doi:10.1007/s12210-010-0102-4, 2010.
- Galli, P.: New empirical relationships between magnitude and distance for liquefaction, *Tectonophysics*, 324, 169–187, 2000.
- Ghelardoni, R.: Osservazioni sulla tettonica trasversale nell'Appennino Settentrionale, *Boll. Soc. Geol. Ital.*, 84, 277–290, 1965.
- Guidoboni, E., Ferrari, G., Mariotti, D., Comastri, A., Tarabusi, G., and Valensise, G.: CFTI4Med, Catalogue of Strong Earthquakes in Italy (461 B.C.–1997) and the Mediterranean Area (760 B.C.–1500), INGV-SGA; available at: <http://storing.ingv.it/cfti4med/>, 2007.
- ISIDE Database: Italian Seismological Instrumental and parametric database, INGV, <http://iside.rm.ingv.it>, 2012.
- ISPRA: Geological effects induced by the seismic sequence started on May 20, 2012, in Emilia ($M_w=5.9$), Preliminary Report, Dipartimento Difesa del Suolo, SGI, Roma, 31 May 2012, <http://www.isprambiente.gov.it/files/progetti/inqua/inqua-primo-rapporto-emilia-2012.pdf/view>, 2012.
- Marcaccio, M. and Martinelli, G.: Effects on the groundwater levels of the May–June 2012 Emilia seismic sequence, *Ann. Geophys.*, 55, 811–814, doi:10.4401/ag-6139, 2012.
- Montone, P., Mariucci, M. T., and Pierdominici, S.: The Italian present-day stress map, *Geophys. J. Int.*, 189, 705–716, doi:10.1111/j.1365-246X.2012.05391.x, 2012.
- Obermeier, S. F.: Use of liquefaction-induced features for paleoseismic analysis – An overview of how seismic liquefaction features can be distinguished from other features and how their regional distribution and properties of source sediment can be used to infer the location and strength of Holocene paleo-earthquakes, *Eng. Geol.*, 44, 1–76, 1996.
- Pesci, A., Casula, G., and Boschi, E.: Laser scanning the Garisenda and Asinelli towers in Bologna (Italy): detailed deformation patterns of two ancient leaning buildings, *J. Cult. Herit.*, 12, 117–127, 2011.
- Pesci, A., Casula, G., Teza, G., Bonali, E., and Boschi, E.: Strategy for the detection of vertical movements in historical environments from fast high-precision GPS measurements, *J. Geophys. Eng.*, 9, 230, doi:10.1088/1742-2132/9/2/230, 2012.
- Pezzo, G., Merryman Boncori, J. P., Tolomei, C., Salvi, S., Atzori, S., Antonioli, A., Trasatti, E., Novali, F., Serpelloni, E., Candela, L., and Giuliani, R.: Coseismic deformation and source modeling of the May 2012 Emilia (Northern Italy) earthquakes, *Seismol. Res. Lett.*, in review, 2013.
- Pieri, M. and Groppi, G.: Subsurface geological structure of the Po plain, Italy, *Pubbl. 414, Cons. Naz. Delle Ric., Agip, Rome, Progetto Finalizzato Geodinamica*, 414, 1981.
- Pondrelli, S., Salimbeni, S., Perfetti, P., and Danecek P.: Quick regional centroid moment tensor solutions for the Emilia 2012 (northern Italy) seismic sequence, *Ann. Geophys.*, 55, 615–621, doi:10.4401/ag-6146, 2012.
- Regione Emilia-Romagna: Primo rapporto sugli effetti della liquefazione osservati a S. Carlo, frazione di S. Agostino (Provincia di Ferrara), A cura del gruppo di lavoro per la valutazione degli effetti di liquefazione a seguito dei terremoti del 20 e 29 maggio 2012 (Regione Emilia-Romagna, PG. 2012.0134978 del 31/5/2012), Bologna, 25 June 2012, http://ambiente.regione.emilia-romagna.it/geologia/temi/sismica/liquefazione-gruppo-dilavoro/rapporto_sancarolo.pdf, 2012.
- Regione Emilia-Romagna and ENI-AGIP: Riserve idriche sotterranee della Regione Emilia-Romagna, edited by: Di Dio, G., S.EL.CA., Firenze, 120 pp., 1998.
- Rovida, A., Camassi, R., Gasperini, P., and Stucchi, M. (Eds.): CPTI11, the 2011 version of the Parametric Catalogue of Italian Earthquakes, Milano, Bologna, <http://emidius.mi.ingv.it/CPTI>, 2011.
- Salvi, S., Tolomei, C., Merryman Boncori, J. P., Pezzo, G., Atzori, S., Antonioli, A., Trasatti, E., Giuliani, R., Zoffoli, S., and Colletta, A.: Activation of the SIGRIS monitoring system for ground deformation mapping during the Emilia 2012 seismic sequence, using COSMO-SkyMed InSAR data, *Ann. Geophys.*, 55, 797–802, doi:10.4401/ag-6181, 2012.
- Scognamiglio, L., Margheriti, L., Mele, F. M., Tinti, E., Bono, A., De Gori, P., Lauciani, V., Lucente, F. P., Mandiello, A. G., Marocci, C., Mazza, S., Pintore, S., and Quintiliani, M.: The 2012 Pianura Padana Emiliana seismic sequence: locations, moment tensors and magnitudes, *Ann. Geophys.*, 55, 549–559, doi:10.4401/ag-6159, 2012.
- TDMT Database: Real-time determination of seismic moment tensor for the Italian region, INGV, <http://cnt.rm.ingv.it/tgmt.html>, 2012.
- Tertulliani, A., Arcoraci, L., Berardi, M., Bernardini, F., Brizuela, B., Castellano, C., Del Mese, S., Ercolani, E., Graziani, L., Maramai, A., Rossi, A., Sbarra, M., and Vecchi, M.: The Emilia 2012 sequence: a macroseismic survey, *Ann. Geophys.*, 55, 679–687, doi:10.4401/ag-6140, 2012.
- Tuttle, M. P.: The use of liquefaction features in paleoseismology: Lessons learned in the New Madrid seismic zone, central United States, *J. Seismol.*, 5, 361–380, 2001.
- Tuttle, M. P., Schweig, E. S., Sims, J. D., Lafferty, R. H., Wolf, L. W., and Haynes, M. L.: The earthquake potential of the New Madrid seismic zone, *Bull. Seism. Soc. Am.*, 92, 2080–2089, 2002.
- Uni Insubria: Earthquake environmental effects accompanying the May 20, 2012, Finale Emilia earthquake; preliminary report, First report, 29 May 2012, DipSAT Uni Insubria Como, edited by: Berlusconi, A., Livio, F., Ferrario, F., Gambillara, R. and Michetti, A. M., 2012.